

A Porphyrin-Based Discrete Tetragonal Prismatic Cage: Host–Guest Complexation and Its Application in Tuning Liquid-Crystalline Behavior

Guocan Yu,* Yang Ye, Zaizai Tong,* Jie Yang, Zhengtao Li, Bin Hua, Li Shao, Shijun Li*

The host–guest complexation between a porphyrin-based 3D tetragonal prism (**H**) and electron-rich pyrene is investigated. This host–guest molecular recognition is further utilized to suppress the liquid-crystalline behavior of a nematic molecule (**G**) containing cyanobiphenyl mesogens functionalized with a pyrenyl unit. Furthermore, coronene, with an increased number of π -electrons, is used as a competitive guest to recover the liquid-crystalline behavior of **G**. This supramolecular approach provides a glimpse of the new possibilities to modulate the structures of the mesophases.



1. Introduction

Self-organization has opened up new and exciting perspectives in the design and engineering of novel, controllable architectures on the nano- and mesoscopic length scales.^[1] Liquid-crystalline (LC) materials self-organize

from mesogens into complicated, hierarchical structures with mobile and ordered states.^[2] Functional liquid-crystal assemblies are unique vehicles for the development of nano- and mesoscopic engineered materials with attractive properties, including information and mass transport, templates, catalysis, sensing, and electro-optical displays.^[3] In order to enrich the functional capabilities of LCs and enable their applications in various fields, it is important to develop novel strategies to tune LC behaviors. In contrast to conventional covalent approaches to regulate LC materials that have a deleterious effect on their performance and durability, supramolecular strategies encompassing dynamic and reversible interactions offer distinct advantages in the tuning of LC properties.^[4] Along these lines, supramolecular LC assemblies can be built upon specific noncovalent interactions, such as hydrogen bonds, ionic bonds, and charge-transfer interactions, ultimately resulting in dynamically functional materials.^[5] Among various supramolecular approaches, host–guest recognition has become particularly attractive due to its excellent stimuli-responsive nature.

Coordination-driven self-assembly is a powerful method to fabricate supramolecular coordination complexes (SCCs) via the spontaneous formation of

Dr. G. Yu, J. Yang, Z. Li, B. Hua, L. Shao
State Key Laboratory of Chemical Engineering
Department of Chemistry
Zhejiang University
Hangzhou 310027, P. R. China
E-mail: guocanyu@zju.edu.cn

Y. Ye, Prof. S. Li
College of Material
Chemistry and Chemical Engineering
Hangzhou Normal University
Hangzhou 310036, P. R. China
E-mail: l_shijun@hznu.edu.cn

Dr. Z. Tong
Department of Materials Engineering
College of Materials and Textile
Zhejiang Sci-Tech University
Hangzhou 310028, P. R. China
E-mail: tongzz@zstu.edu.cn

metal–ligand bonds that result in a single thermodynamically favored product.^[6] This increasingly popular methodology enables a combinatorial molecular library consisting of complementary, rationally designed organic ligands and metal containing precursors that may be combined to afford specific discrete assemblies.^[7] Well-defined cavity-cored 2D metallacycles and 3D metallacages have been prepared through coordination-driven self-assembly approaches. These scaffolds can be easily functionalized on their interior or exterior surfaces for applications including host–guest chemistry, molecular flasks, catalysis, bioengineering, and amphiphilic self-assembly.^[8] The use of metal–ligand bonding affords control over both directionality and stoichiometry due to the predictable and well-defined coordination geometries of transition metal ions. The incorporation of SCCs into LC materials introduces the possibility of additional intermolecular interactions, such as metal–metal, metal–ligand, and host–guest interactions, resulting in a rich chemistry.^[5c,9] For example, Donnio and co-workers reported the supramolecular organization of a new family of LC host–guest complexes based on an arene ruthenium metallacycle and LC dendrimers.^[5c] By employing host–guest recognition, interesting LC behaviors were achieved in their supramolecular systems.

Herein, a porphyrin-based 3D tetragonal prism (**H**) was obtained from the multicomponent coordination-driven self-assembly of two different donors (**1** and **3**) and *cis*-(PEt₃)₂Pt(OTf)₂ (**2**) under stoichiometric control. These building blocks **1**, **2**, and **3** act as the faces, vertices, and pillars of the metallacage, respectively. This tetragonal prismatic cage was then utilized as a host to complex with electron-rich pyrene (**P**) driven by face-to-face $\pi\cdots\pi$ stacking and orthogonal C–H $\cdots\pi$ interactions. Based on this host–guest recognition motif, **H** was employed to tune the LC behavior of a smectic molecule (**G**) containing cyanobiphenyl mesogens functionalized with a pyrenyl unit. The mesomorphism of **G** was suppressed in the presence of **H**, because of the lack of $\pi\cdots\pi$ stacking interactions between the pyrenyl groups and additional electrostatic repulsions between the metallacages arising from the host–guest complexation. Moreover, the LC properties of **G** were recovered upon addition of coronene, due to a competitive complexation.

2. Experimental Section

2.1. Materials and Methods

2.1.1. General Methods

1-(3'-Dimethylaminopropyl)-3-ethylcarbodiimide hydrochloride, dimethyl 5-hydroxyisophthalate, 4-dimethylaminopyridine, and other reagents were commercially available and used as received.

¹H NMR and ¹³C NMR spectra were recorded on a Bruker Avance III-400 spectrometry. Matrix-assisted laser desorption/ionization time-of-flight (MALDI-TOF) mass spectrometry was performed on an ultrafleXtreme MALDI-TOF system. HRMS were obtained on a WATERS GCT Premier mass spectrometer. The melting points were collected on an SHPSIC WRS-2 automatic melting point apparatus. Differential scanning calorimetry experiments were conducted on a DSCQ1000 thermal analysis instrument under N₂ at a rate of 10 °C min⁻¹. Polarized optical microscopy observations at various thermal conditions were carried out on an Olympus microscope (BX51) equipped with a hot stage. The wavelength of X-ray was 1.24 Å, and the sample-to-detector distance was set as 1900 and 255 mm for small- (SAXS) and wide-angle X-ray scattering (WAXS) measurement, respectively. 2D SAXS/WAXS patterns at various temperatures were recorded. The average exposure time was 50 s for each scan. Bull tendon and cerium oxide were used as standard material for calibrating the SAXS and WAXS scattering vector, respectively. The 2D SAXS/WAXS patterns were converted into 1D SAXS/WAXS profiles using Fit2D software.

2.1.2. Sample Preparation for Thermal Investigations

G was dissolved in CH₂Cl₂. One drop of the sample solution was placed on a glass surface, the solvent was evaporated at room temperature, and the sample was dried under vacuum. Before thermal experiments were carried out, the samples were heated into the isotropic liquid under N₂ protection and annealed for 15 min. Then the samples were cooled down very slowly to the room temperature.

For the host–guest complex **H**⊃**G**, the building blocks (**H** and **G**, molar ratio was 1:1) were added into CH₂Cl₂ and stirred overnight. One drop of the sample solution was placed on a glass surface, the solvent was evaporated at room temperature, and the sample was dried under vacuum. Before thermal experiments were carried out, the samples were heated to 200 °C under N₂ protection and annealed for 15 min. Then the samples were cooled down very slowly to the room temperature.

For the ternary system, coronene (1.2 equiv.) was added into the CH₂Cl₂ solution of **H**⊃**G** and stirred at room temperature overnight. The resultant solution was injected into acetonitrile and stirred for 2 h, the formed precipitation was filtered off. The precipitation was dissolved in CH₂Cl₂ again, and the dissolution–precipitation process repeated five times. The obtained solid was dissolved in CH₂Cl₂. One drop of the sample solution was placed on a glass surface, the solvent was evaporated at room temperature and the sample was dried under vacuum. Before thermal experiments were carried out, the samples were heated into the isotropic liquid under N₂ protection and annealed for 15 min. Then the samples were cooled down very slowly to the room temperature.

3. Results and Discussion

Prism **H** was prepared by mixing 90° Pt(II) acceptor **2**, carboxylate ligand **3**, and tetrapyrrolylporphyrin (**1**) in a ratio of 8:4:2.^[10] The host–guest complexation between **H** and

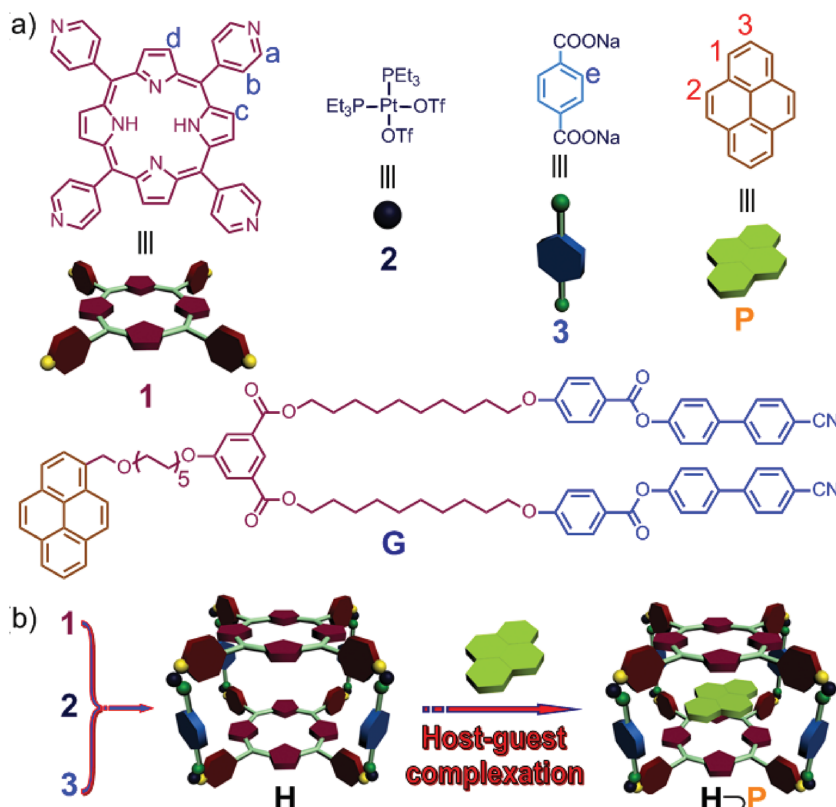


Figure 1. a) Chemical structures and cartoon representations of the building blocks (1, 2, 3, P, and G). b) Schematic representation of the host–guest complexation between H and P.

P was investigated by ^1H NMR spectroscopy. As shown in Figure 1b, the signals related to the protons H_1 , H_2 , and H_3 on P shifted upfield upon addition of H ($\Delta\delta = -0.058$, -0.069 , and -0.052 ppm for H_1 , H_2 , and H_3 , respectively), indicating that these protons are located within the cavity of H upon the formation of an inclusion complex between H and P. Moreover, the signals corresponding to the protons on H exhibited slight chemical shift changes due to host–guest interactions.^[10] 2D nuclear Overhauser effect spectroscopy (NOESY) NMR spectroscopy, a useful tool to study the relative positions of the components in host–guest inclusion complexes, was utilized to investigate the complexation between H and P. Nuclear Overhauser effect (NOE) correlations were observed between the signals related to protons H_3 on P and protons (H_b and H_c) on H (Figure S12, Supporting Information), suggesting that planar P was located within the cavity of H.

The host–guest complexation between H and P was further supported by electrospray ionization time-of-flight mass spectrometry (ESI-TOF-MS). As shown in Figure 2d–f, the isotopically resolved peaks corresponding to $\text{H}\supset\text{P}$ with the loss of OTf^- anions were found at m/z 1535.6 [$\text{H}\supset\text{P} - 4\text{OTf}$] $^{4+}$, 1582.9 [$\text{H}\supset\text{P} - 3\text{OTf} + \text{K}$] $^{4+}$, and 2097.5 [$\text{H}\supset\text{P} - 3\text{OTf}$] $^{5+}$. All of these peaks were isotopically resolved and agreed very well with their calculated theoretical

distributions, which confirm the formation of a 1:1 host–guest complex between H and P. These results are consistent with those obtained from NMR titration experiments (Figure S13–S15, Supporting Information). To estimate the association constant for the complexation between H and P, ^1H NMR titrations were conducted (Figure S13, Supporting Information). A mole ratio plot based on the titration experiments demonstrated that the complexation of H with P had a 1:1 stoichiometry (Figure S15, Supporting Information). The association constant (K_a) was calculated to be $78.6 \pm 8.1 \text{ M}^{-1}$ as determined from a nonlinear curve-fitting (Figure S14, Supporting Information).

With this new recognition motif between H and P established, the cage was then investigated for its effects on the LC behavior of G functionalized with a pyrenyl unit. Diffusion ordered NMR spectroscopy (DOSY) experiments were performed to verify the complexation between H and G (Figure S19–S22, Supporting Information). The measured weight average diffusion coefficients (D) of H and G were found to be 3.63×10^{-10} and $4.16 \times 10^{-10} \text{ m}^2 \text{ s}^{-1}$, respectively. However, a decrease of D was observed for each component of the system when they were mixed together in solution ($D = 1.80 \times 10^{-10} \text{ m}^2 \text{ s}^{-1}$), implying that the proposed $\text{H}\supset\text{G}$ complex was larger than its precursors.

The LC behavior and thermal properties of G were investigated by polarized optical microscopy (POM) and differential scanning calorimetry (DSC). Three DSC thermograms were collected (heating, cooling, second heating) after the sample was annealed at 200°C so as to eliminate any thermal history (Figure S23, Supporting Information). The glass transition (T_g) and isotropization temperature (T_i) of G were determined to be 23 and 107°C , respectively, revealing a relatively wide temperature range smectic A (SmA) LC mesophase. Furthermore, the supercooling of the sample was measured to be 11°C (Figure S23, Supporting Information). Interestingly, a disappearance of the melting peaks from the second heating scan was detected, mainly due to the extremely slow crystallization of G as evidenced by the lack of a crystallization peak during cooling scans (Figure S23, Supporting Information). The mesophase was identified by POM from the formation of a typical focal-conic fan texture (100°C , Figure 4a), indicative of untilted lamellae. When the temperature was increased to 180°C , which was higher than

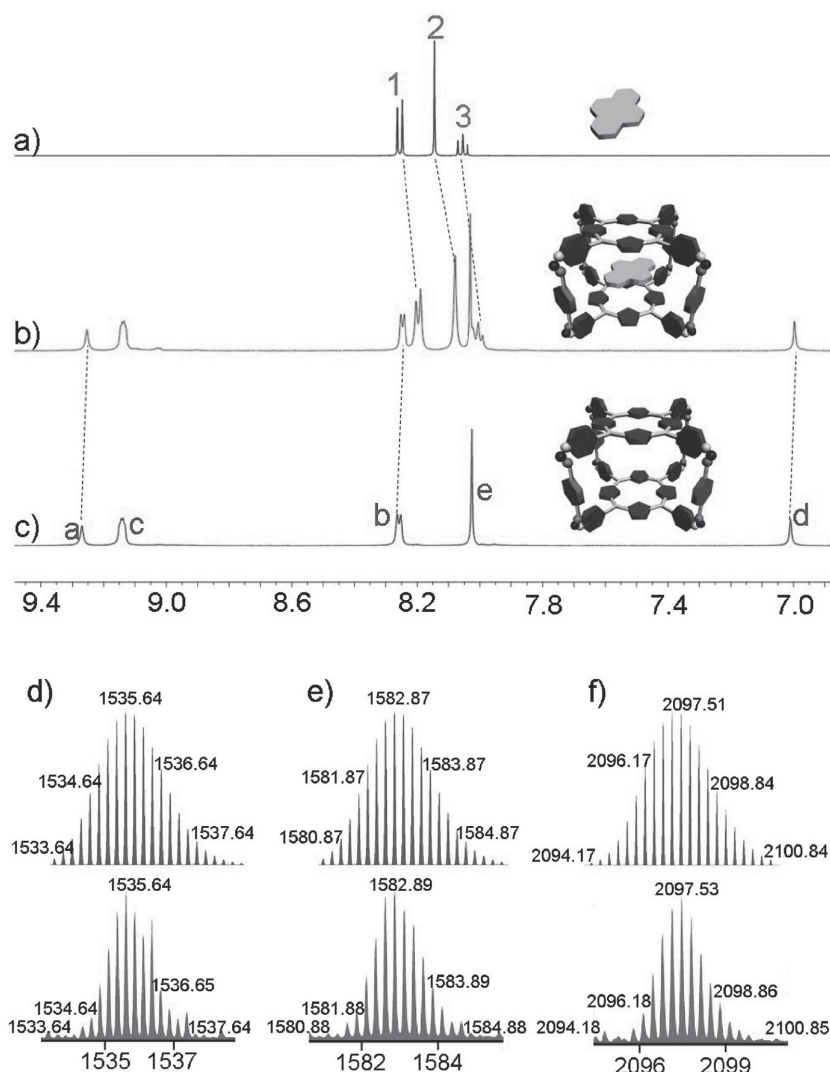


Figure 2. ^1H NMR spectra (400 MHz, CD_2Cl_2 , room temperature): a) **P** (6.00×10^{-3} M), b) **P** (6.00×10^{-3} M) and **H** (2.00×10^{-3} M), and c) **H** (2.00×10^{-3} M). Experimental (red) and calculated (blue) ESI-TOF-MS spectra of **H>P**: d) [**H>P** – 4OTf] $^{4+}$, e) [**H>P** – 3OTf + K] $^{4+}$, and f) [**H>P** – 3OTf] $^{3+}$.

the T_i , the focal-conic fan textures disappeared completely as the packing of the cyanobiphenyl mesogenic moieties changed from an anisotropic state to an isotropic state. In addition, the LC behavior of **G** was recovered after decreasing the temperature to 80 °C, which was lower than the T_i . It should be noted that coexistence of crystalline and LC states was observed in the POM image when the temperature was 40 °C (Figure 4a), which was consistent with the result obtained from DSC (the first heating scan, Figure S23, Supporting Information). The formation of a crystalline phase may be associated with the long annealing time of **G** during preparation process.

The arrangement of the mesogenic molecules was studied by temperature-dependent SAXS/WAXS analyses (Figure 3a,b). As shown in Figure 3a, crystalline diffraction reflections were monitored in the low-angle and

large-angle regions at low temperature (40 °C), indicating partial crystalline character of the samples, which was consistent with the result obtained from POM (40 °C, Figure 4a) and DSC (Figure S23, Supporting Information). When the temperature increased to 100 °C, two sharp maxima in the low-angle region were detected. For the two low-angle maxima, their reciprocal spacing ratio is 1:2 corresponding to the first (001) and second (002) order reflections from the smectic layers, characteristic of a classical smectic A phase.^[4c] The periodicity (d) was deduced to be 5.7 nm by $d = 2\pi/q$. It should be noted that the intensity of peak (001) was almost identical to that of (002), suggesting that there was a central layer of electron-rich containing units, between the two mesogenic sublayers. This central layer was likely formed by the pyrene rings and the phenyl rings of the hydroxyisophthalic units, which was commonly observed with mesomorphic compounds built with polar mesogens, such as cyanobiphenyls.^[13b] At this temperature (100 °C), the crystalline planes disappeared due to the melting of the crystals of **G** (Figure 3b). Additionally, the classical wide-angle broad scattering with a maximum at $\approx 4.2\text{--}5.0$ Å resulting from the overlapping distances between molten aliphatic chains, aromatic rings, and mesogens, respectively, were also observed, even when the temperature reached 180 °C (Figure 3b).^[5c] Based on previous reports

of LC compounds fabricated from similar cyanobiphenyl mesogenic moieties and the corresponding SAXS/WAXS investigations,^[4c] a possible model for the supramolecular organization of **G** within the smectic A phase is proposed (Figure 4e). **G**, containing two cyanobiphenyl mesogenic units, is statistically oriented upward and downward with the pyrene units in the middle. This alternating structure creates a modulation of the electron density with a period equal to half the full layer thickness. When the temperature was further increased to 180 °C, higher than the T_i , the two sharp reflections observed at small angles disappeared, confirming a transition from the LC state to an isotropic liquid. Reversibly, the first and second-order reflections reappeared upon decreasing the temperature to 80 °C, in line with the POM investigations. It should be emphasized that the reflections in the low-angle region

were a little broader when the sample was cooled to 80 °C. The reason was that the arrangement of **G** could not recover to the highly ordered layered structure at this temperature in a short time, which was confirmed by DSC studies showing a relative wide exothermic peak around 96 °C in the cooling run.

More interestingly, the LC behavior of **G** disappeared upon addition of **H**. As shown in Figure S23 (Supporting Information), the isotropization temperature of **G** in the presence of **H** vanished during the heating–cooling cycle. In sharp contrast to the result of free **G**, no reflections were detected in the temperature-dependent small-angle range for **H**⊃**G** (Figure 3c), confirming that the layered structure of the mesophase transformed into a disordered isotropic state due to the host–guest complexation between **H** and the pyrenyl group grafted onto **G** (Figure 4d). The reason for this transformation is that the tetragonal prismatic cages are much larger than the mean size of the mesogenic moieties, resulting in the suppression of mesomorphism. The electrostatic repulsion arising from the metallacages was not conducive to an ordered packing of **H**⊃**G**, which might be another factor governing the disappearance of LC behavior. Moreover, the lack of $\pi\cdots\pi$ stacking interactions between the pyrenyl groups arising from the formation of **H**⊃**G** was responsible for the suppression of mesomorphism. This phenomenon was also confirmed by temperature-dependent POM investigations. In contrast to the POM observations for free **G**, only small spots were observed and no changes were found during the cooling or heating processes for **H**⊃**G** (Figure 4b), originating from the host–guest complexes. WAXS patterns recorded at 40 and 100 °C revealed that new and complicated wide-angle signals were monitored upon host–guest complexation, which were different from those of free **H** and free **G**. However, it was impossible to extract precise arrangement of the host–guest complexes in this binary supramolecular system. As shown in Figure 3d, there existed several reflections in the large-angle region for free **H**, indicating that the rigid metallacage possessed crystallinity. Spots were observed in temperature-dependent POM images even

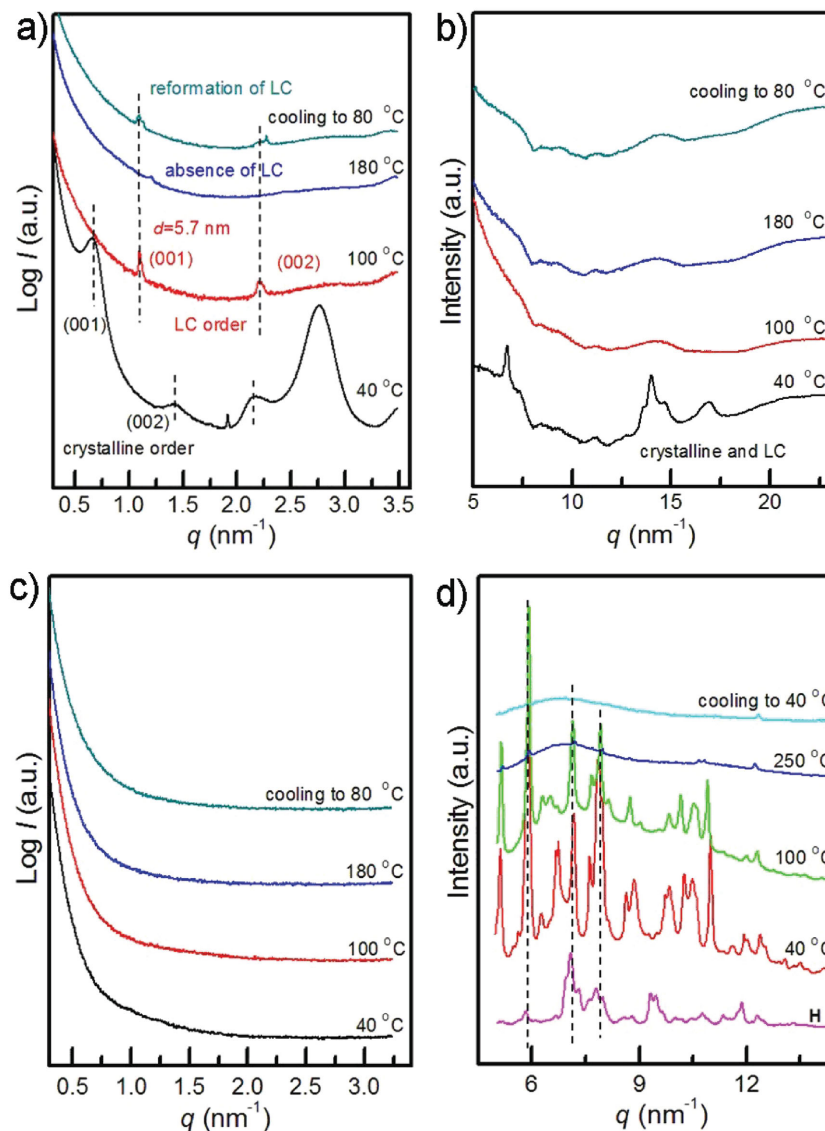


Figure 3. a) Lorenz-corrected SAXS and b) WAXS profiles of **G** at indicated temperatures. c) Lorenz-corrected SAXS profiles of **H**⊃**G** at indicated temperatures. d) WAXS profiles of **H** at room temperature and **H**⊃**G** at indicated temperatures.

the temperature was increased to 220 °C (Figure 4d). From comparison of Figure 4b,d, we found that the morphologies and sizes of the spots were quite different, further demonstrating that the spots in Figure 4b generated from **H**⊃**G**. Some information about the thermostability of the metallacage was acquired from WAXS profiles and thermal gravimetric analysis (TGA). Figure 3d revealed that the reflections in the large-angle regions vanished at 250 °C and never recovered to their original state, ascribed to the decomposition of the compounds. Furthermore, TGA of **H** indicated that decomposition took place when the temperature increased to 250 °C (Figure S24, Supporting Information), which was also in accordance with the WAXS result.

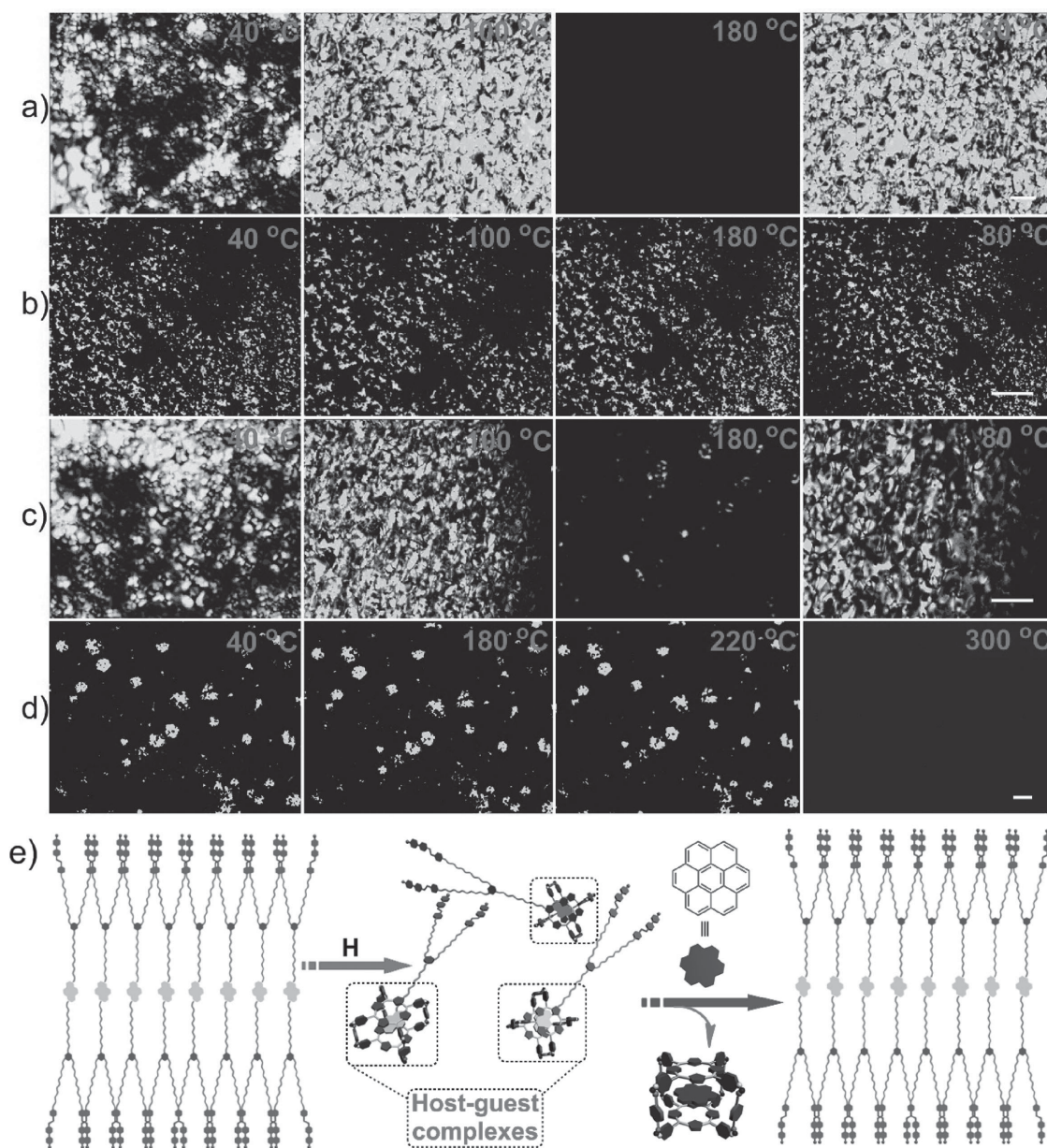


Figure 4. Thermal POM images of a) **G**, b) **H>G**, and c) **H>G** in the presence of coronene at different temperatures. The scale bar is 50 μm . Cartoon representation of the supramolecular method tuning the LC behaviors of **G** through host–guest complexation.

Arguably the most striking feature of supramolecular chemistry is that noncovalent interactions are dynamic and reversible, endowing supramolecular systems with excellent stimuli-responsive characteristics.^[11] From computational simulations of **H**, we established that the width of **H** was about 13.7 Å (Figure S25, Supporting Information), which was larger than the radius of coronene (11.9 Å in van der Waals radii, Figure S26, Supporting Information). As such, it was envisioned that metallacage **H** could be used as a host for coronene. Compared with pyrene, the larger polycyclic aromatic coronene molecule has an increased number of π -electrons

and thus could form a more stable host–guest complex with **H** due to its stronger face-to-face $\pi\cdots\pi$ stacking and orthogonal C–H $\cdots\pi$ interactions.^[12] The association constant between **H** and coronene in dichloromethane- d_2 was determined to be $278 \pm 22 \text{ M}^{-1}$ (Figure S16–S18, Supporting Information), which was about three times that of **H>P**. Therefore, coronene could act as a competitive guest to recover the LC behavior of this system, arising from the disassociation of the host–guest complexation between **H** and **G**. The resultant **H>coronene** could be eliminated from this ternary system due to the discrepancy in solubility between **H>coronene** and **G** in

acetonitrile. POM observations confirmed the recovery of the LC behavior of **G**. Focal-conic fan textures observed at 100 °C and almost disappeared at 180 °C (Figure 4c). These temperature-dependent changes were reversible, and the focal-conic fan textures reappeared when the mixture was cooled to 80 °C. It should be noted that spherical spots existed even when the temperature was higher than the T_i of **G**, which was ascribed to the poor solubility of the remaining **H** coronene that resulted in phase separation or crystallization.

4. Conclusion

In summary, we have investigated the host-guest recognition chemistry between a porphyrin-based discrete platinum(II) metallacage (**H**) and π -electron-rich guests (pyrene and coronene). The recognition between **H** and **P** was utilized to suppress the mesomorphism of **G**. These effects were attributed to the large size of the hosts along with the lack of π – π stacking interactions between the pyrenyl groups and the introduction of electrostatic repulsion between the complexed metallacages. The system demonstrated the dynamic and reversible nature of noncovalent interactions upon the addition of coronene as a competitive guest that interrupted the host-guest interactions between **H** and **G**. Once **G** was freed, it re-established its LC behavior. This supramolecular strategy to tunable LC materials offers a new method to modulate the structures of mesophases, which can be applied in various fields, including optoelectronics, liquid-crystalline polymers, electro-optical displays, and sensors.^[13]

Supporting Information

Supporting Information is available from the Wiley Online Library or from the author.

Acknowledgements: This work was supported by the Fundamental Research Funds for the Central Universities and the National Natural Science Foundation of China (21072039).

Received: May 13, 2016; Revised: June 3, 2016;
Published online: July 28, 2016; DOI: 10.1002/marc.201600280

Keywords: coordination-driven self-assembly; host-guest systems; liquid crystalline; self-organization; supramolecular chemistry

- [1] a) L.-J. Wan, *Acc. Chem. Res.* **2006**, *39*, 334; b) B. H. Northrop, Y.-R. Zheng, K.-W. Chi, P. J. Stang, *Acc. Chem. Res.* **2009**, *42*, 1554.

- [2] a) G. Ungar, Y. Liu, X. Zeng, V. Percec, W.-D. Cho, *Science* **2003**, *299*, 1208; b) B. Donnio, S. Buathong, I. Bury, D. Guillon, *Chem. Soc. Rev.* **2007**, *36*, 1495; c) B. Zhuang, Z.-G. Wang, *Macromolecules* **2012**, *45*, 6220; d) E.-K. Fleischmann, R. Zentel, *Angew. Chem. Int. Ed.* **2013**, *52*, 8810.
- [3] a) T. Kato, N. Mizoshita, K. Kishimoto, *Angew. Chem. Int. Ed.* **2006**, *45*, 38; b) J. Etxebarria, M. B. Ros, *J. Mater. Chem.* **2008**, *18*, 2919; c) H. K. Bisoyi, S. Kumar, *Chem. Soc. Rev.* **2011**, *40*, 306.
- [4] a) I. M. Saez, J. W. Goodby, *J. Mater. Chem.* **2005**, *15*, 26; b) T. Kajitani, Y. Suna, A. Kosaka, T. Osawa, S. Fujikawa, M. Takata, T. Fukushima, T. Aida, *J. Am. Chem. Soc.* **2013**, *135*, 14564; c) S. Mula, S. Frein, V. Russo, G. Ulrich, R. Ziessel, J. Barbera, R. Deschenaux, *Chem. Mater.* **2015**, *27*, 2332.
- [5] a) T. Kajitani, H. Onouchi, S.-I. Sakurai, K. Nagai, K. Okoshi, K. Onitsuka, E. Yashima, *J. Am. Chem. Soc.* **2011**, *133*, 9156; b) N. D. Suhan, S. J. Loeb, S. H. Eichhorn, *J. Am. Chem. Soc.* **2013**, *135*, 400; c) A. Pitto-Barry, N. P. E. Barry, V. Russo, B. Heinrich, B. Donnio, B. Therrien, R. Deschenaux, *J. Am. Chem. Soc.* **2014**, *136*, 17616; d) S. Pan, M. Ni, B. Mu, Q. Li, X.-Y. Hu, C. Lin, D. Chen, L. Wang, *Adv. Funct. Mater.* **2015**, *25*, 3571.
- [6] a) M. Fujita, M. Tominaga, A. Hori, B. Therrien, *Acc. Chem. Res.* **2005**, *38*, 369; b) A. Pitto-Barry, N. P. E. Barry, O. Zava, R. Deschenaux, B. Therrien, *Chem. Asian J.* **2011**, *6*, 1595; c) A. Pitto-Barry, N. P. E. Barry, O. Zava, R. Deschenaux, P. J. Dyson, B. Therrien, *Chem. Eur. J.* **2011**, *17*, 1966; d) T. R. Cook, Y.-R. Zheng, P. J. Stang, *Chem. Rev.* **2013**, *113*, 734; e) J. G. Hardy, *Chem. Soc. Rev.* **2013**, *42*, 7881; f) X. Yan, T. R. Cook, P. Wang, F. Huang, P. J. Stang, *Nat. Chem.* **2015**, *7*, 342; g) Y. Ye, T. R. Cook, S.-P. Wang, J. Wu, S. Li, P. J. Stang, *J. Am. Chem. Soc.* **2015**, *137*, 11896.
- [7] a) S. Li, J. Huang, T. R. Cook, J. B. Pollock, H. Kim, K.-W. Chi, P. J. Stang, *J. Am. Chem. Soc.* **2013**, *135*, 2084; b) X. Yan, T. R. Cook, J. B. Pollock, P. Wei, Y. Zhang, Y. Yu, F. Huang, P. J. Stang, *J. Am. Chem. Soc.* **2014**, *136*, 4460; c) T. R. Cook, P. J. Stang, *Chem. Rev.* **2015**, *115*, 7001.
- [8] a) Y.-R. Zheng, Z. Zhao, M. Wang, K. Ghosh, J. B. Pollock, T. R. Cook, P. J. Stang, *J. Am. Chem. Soc.* **2010**, *132*, 16873; b) A. Pitto-Barry, O. Zava, P. J. Dyson, R. Deschenaux, B. Therrien, *Inorg. Chem.* **2012**, *51*, 7119; c) X. Yan, S. Li, T. R. Cook, X. Ji, Y. Yao, J. B. Pollock, Y. Shi, G. Yu, J. Li, F. Huang, P. J. Stang, *J. Am. Chem. Soc.* **2013**, *135*, 14036; d) L.-J. Chen, G.-Z. Zhao, B. Jiang, B. Sun, M. Wang, L. Xu, J. He, Z. Abliz, H. Tan, X. Li, H.-B. Yang, *J. Am. Chem. Soc.* **2014**, *136*, 5993.
- [9] a) P. D. Frischmann, S. Guieu, R. Tabeshi, M. MacLachlan, *J. Am. Chem. Soc.* **2010**, *132*, 7668; b) P. Dechambenoit, S. Ferlay, B. Donnio, D. Guillon, M. W. Hosseini, *Chem. Commun.* **2011**, *47*, 734; c) A. M. Prokhorov, A. Santoro, J. A. G. Williams, D. W. Bruce, *Angew. Chem. Int. Ed.* **2012**, *51*, 95; d) E. Terazzi, G. Rogez, J.-L. Gallani, B. Donnio, *J. Am. Chem. Soc.* **2013**, *135*, 2708.
- [10] a) Y.-R. Zheng, Z. Zhao, H. Kim, M. Wang, K. Ghosh, J. B. Pollock, K.-W. Chi, P. J. Stang, *Inorg. Chem.* **2010**, *49*, 10238; b) Y.-R. Zheng, W.-J. Lan, M. Wang, T. R. Cook, P. J. Stang, *J. Am. Chem. Soc.* **2011**, *133*, 17045.
- [11] a) D.-W. Yoon, D. E. Gross, V. M. Lynch, J. L. Sessler, B. P. Hay, C.-H. Lee, *Angew. Chem. Int. Ed.* **2008**, *47*, 5038; b) Z. Niu, H. W. Gibson, *Chem. Rev.* **2009**, *109*, 6024; c) C. Talotta, C. Gaeta, Z. Qi, C. A. Schalley, P. Neri, *Angew. Chem. Int. Ed.* **2013**, *52*, 7437; d) G. Yu, K. Jie, F. Huang, *Chem. Rev.* **2015**, *115*, 7240; e) K. Zhu, C. A. O'Keefe, V. N. Vukotic, R. W. Schurko, S. J. Loeb, *Nat. Chem.* **2015**, *7*, 514.

- [12] E. J. Dale, N. A. Vermeulen, A. A. Thomas, J. C. Barnes, M. Juricek, A. K. Blackburn, N. L. Strutt, A. A. Sarjeant, C. L. Stern, S. E. Denmark, J. F. Stoddart, *J. Am. Chem. Soc.* **2014**, *136*, 10669.
- [13] a) B. Xu, T. M. Swager, *J. Am. Chem. Soc.* **1993**, *115*, 1159;
b) T. Cardinaels, K. Driesen, T. N. Parac-Vogt, B. Heinrich, C. Bourgogne, D. Guillon, B. Donnio, K. Binnemans, *Chem. Mater.* **2005**, *17*, 6589; c) J. J. Reczek, K. R. Villazor, V. Lynch, T. M. Swager, B. L. Iverson, *J. Am. Chem. Soc.* **2006**, *128*, 7995; d) M. Stępień, B. Donnio, J. L. Sessler, *Angew. Chem. Int. Ed.* **2007**, *46*, 1431; e) I. Aprahamian, T. Yasuda, T. Ikeda, S. Saha, W. R. Dichtel, Isoda, T. Kato, J. F. Stoddart, *Angew. Chem. Int. Ed.* **2007**, *46*, 4675; f) E. D. Baranoff, J. Voignier, T. Yasuda, V. Heitz, J.-P. Sauvage, T. Kato, *Angew. Chem. Int. Ed.* **2007**, *46*, 4680.